A Broadband Graphene Based Multi-Functional mid-THz Polarization Converter

Vinit Singh Yadav, *Graduate Student Member, IEEE*, and Amalendu Patnaik, *Senior Member, IEEE*

***Abstract*—A graphene–based multifunctional polarization converter for the mid–THz band is proposed in this work and its electromagnetic behavior is explained with the help of the physics behind it and the circuital theory. The novelty of the proposed reflector lies in the fact that a linear–to–linear (LL) polarization conversion takes place for a chemical potential in 0.3–0.6 eV and a linear–to–circular (LC) in 0.7–1.0 eV across the mono–layered graphene over a large oblique angle ($\approx 40^{\circ}$) of the incident wave. The fractional 3 dB axial ratio bandwidth in the case of LC polarization conversion is 81%. Moreover, for LL polarization conversion it gives 31% fractional bandwidth for polarization conversion ratio (PCR) more than 85%. The structure maintains a thickness of λ/7.5 and a lattice size of λ/18. The proposed multi–functional polarization converter can act as a promising candidate for THz indoor communication.**

***Index Terms*—Axial ratio, graphene, metasurface, multi-mode polarization converter, THz, unit cell.**

I. Introduction

In THE past few years polarization of EM wave has become a key aspect in communication for hassle free receiving of wave. Keeping in mind there are several approaches have been made to design polarization converters, in the initial days of making EM wave polarizer, they were bulky in nature [1]. In this view, due to constitutive parameter flexibility, light weight and wide frequency band applicability, metasurface has attracted a great attention of the researchers in the last two decade [2], [3], [4], [5]. Since then, different approaches have been made to design a metasurface based absorbers, polarizers, filters, cloacking devices, and wave-front manipulator [3], [6], [7], [8]. The metal based metasurface devices, due to its structural robustness are frequency tunable to a very limited band. The linear–to–circular (LC) polarization converter after incorporating active devices and switching can work upto a certain frequency band. A linear–to–linear (LL) polarization converter has achieved a significant frequency band of tunability after applying switches. Some approach have been made to design polarization switching with the help of p-i-n diode and parasitic capacitance. Multi-mode polarization conversion using PIN diodes have been proposed to push the limit of polarization converters [9]. A circular split ring polarization conversion metasurface (PCM) employing plasmon resonance has achieved cross polarization in the band 2.42–3.52 GHz when the diode is ON and co–polarization in OFF condition [10]. But due to the limited frequency of operation and their integrity issue at higher frequency they are not preferred [11]. To overcome this issue, some material which can work as conductive surface over tuning the temperature and doping i.e. VO_2 and graphene are used [12].

The graphene due to its unique property of change in conductivity with altering its applied biasing has very vast area of interest [13], [14], [15]. The tunable polarization converter, absorbers, filters have been proposed till now. A graphene based metasurface LL polarization converter giving 31.1% have been proposed. A frequency tunable LC polarization converter operating in sub-terahertz frequency regime giving fractional 3 dB axial ratio bandwidth (FARBW) of 46.5% is proposed. A graphene-metal metasurface working as a bi-functional with switchable property to attain the linear to linear and linear to circular polarization state by changing the chemical potential from 0-1.0eV. The bi-functional operating band is from 1.38–1.72 THz [16]. A graphene-VO_2 based metasurface linear to linear polarization converter operating in transmitting and reflecting mode depending on the bias voltage to the graphene and temperature of VO_2 is proposed. In this design two parameters, *viz.* chemical potential and temperature, are variable. The frequency of operation in transmitting state is 3.0-6.0 THz and in reflecting state is 3.76–4.15 THz [17]. The graphene chemical potential and VO_2 are used to control the polarization state of metasurface as LL in transmissive mode and LC in reflective mode [12]. A two layered stacked graphene based 45° transmittive type LL polarization converter is designed. The state of polarization is changed by altering the Fermi level of the graphene [18]. In article [19], a graphene patch metasurface and a graphene hole metasurface based multi-band and bi-functional polarization converter is presented. On altering the chemical potential of graphene layer, the graphene hole and graphene patch based metasurface give LL and LC polarization conversion in the frequency band 2.69-4.19 THz and 4.96-6.52 THz, respectively. But still the research is going on to get a better performance and wide-band multi-functional polarization converter with less design complexity.

In this paper, A multi–functional polarization converter using a graphene based double L-shaped perforated structure on top of a metal (gold) backed substrate (SiO_2) is proposed. The L-shaped perforated structure is made on a uniform mono-layered graphene. An external biasing is given to the graphene layer with respect to the ground layer to change the chemical potential

Manuscript received 9 July 2024; revised 3 August 2024; accepted 6 August 2024. Date of publication 9 August 2024; date of current version 16 August 2024. *(Corresponding author: Amalendu Patnaik.)*

The authors are with the Department of Electronics and Communication Engineering, Indian Institute of Technology, Roorkee 247667, India (e-mail: vinitsingh.iitr@ieee.org; amalendu.patnaik@ece.iitr.ac.in).

Digital Object Identifier 10.1109/JPHOT.2024.3441245

of graphene layer. Upon altering the chemical potential, the structure gives a broadband of LC polarization conversion from 2.9 THz to 6.9 THz with axial ratio below 3 dB for chemical potential of 0.9 eV and it maintains a the bandwidth for 0.7ėV to 1.0 eV. Further altering the chemical potential from 0.3 eV to 0.6 eV, it gives a wide-band of LL polarization conversion and at 0.45eV the fractional polarization conversion is 31.5% over the frequency band from 3.6 THz to 5 THz. Moreover, the polarization converter is giving broadband performance for oblique incidence up to 40°. Due to the lack of facility, the proposed polarization converter is not fabricated, but has been verified with the help of surface current distribution and equivalent circuit model (ECM). Further, the performance of the polarization converter is observed by varying the angle of oblique incidence and Fermi level of graphene. The switchable polarization converters at high frequency find applications in polarization sensor, polarization switches, integrated polarization converters and photo-detectors [20], [21].

The unavailability of the facility of fabrication and measurement at our institute, the paper lacks this part. But, it is possible to fabricate and test the proposed structure by using the established fabrication methods. The proposed structure is so thin that a silicon wafer can be used to provide mechanical support. With the use of the e-gun evaporation technology, a silicon wafer can be developed into the metallic plate at the bottom of the structure. Additionally, a 10 µm thick layer of spin-coated silicon dioxide can be created atop a gold metallic layer [22]. However, it must be subjected to ultraviolet (UV) radiation for an hour at 300 °C. Then, using a chemical vapor deposition process at atmospheric pressure, graphene can be produced and deposited onto the silicon dioxide layer [23]. An ion gel can be deposited on the patterned graphene layer to give equipotential (through biasing) to the graphene layer. Due to its low charge mobility at high frequency, it will not affect the resonance [24].

II. Graphene Layer and Its Conductivity

The properties of single layer graphene can be altered by changing the applied chemical potential, operating temperature, scattering time constant, and operating frequency. The surface conductivity relation is given as [25]:

$$\sigma\left(\omega, E_f, \Gamma, T\right) = \sigma_{inter} + \sigma_{intra} \tag{1}$$

$$\sigma_{intra} = \frac{2k_bTe^2}{\pi\hbar} ln\left(2cosh\frac{E_f}{2k_bT}\right)\frac{i}{(\omega + i\Gamma)} = \frac{\alpha}{-i\omega + \Gamma} \tag{2}$$

$$\sigma_{inter} = \frac{e^2}{4\hbar}\left[H\left(\frac{\omega}{2}\right) + i\frac{4\omega}{\pi}\int_0^{\infty}\frac{H\left(\Omega\right) - H\left(\frac{\omega}{2}\right)}{\omega^2 - 4\Omega^2}d\left(\Omega\right)\right] \tag{3}$$

where

$$H\left(\Omega\right) = sinh\left(\frac{\hbar\Omega}{k_bT}\right) / \left[cosh\frac{\hbar\Omega}{k_bT} + cosh\left(\frac{E_f}{k_bT}\right)\right]$$

e, τ, and Γ are the charge, scattering constant, and scattering rate of electron, respectively. The T is temperature and ω is the angular frequency in the operating band.

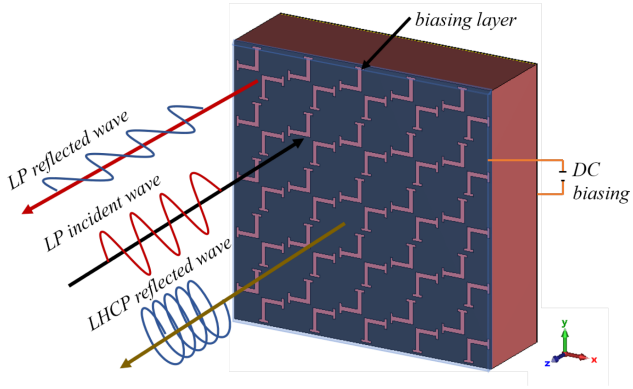

Fig. 1. Schematic view of the proposed graphene based metasurface polarization converter.

$$E_f = \hbar v_f\sqrt{\frac{\pi\varepsilon_d\varepsilon_0 V_g}{et_2}} \tag{4}$$

$v_f = 10^6$m/s is the Fermi velocity, V_g is the potential applied, $\varepsilon_d = 2.2$ is for SiO_2. Drude's conductivity formula for surface conductivity of graphene:

$$\sigma_g\left(\omega\right) = \frac{e^2E_f}{\pi\hbar}\frac{i}{(\omega + i\tau^{-1})} \tag{5}$$

The relative permittivity of graphene, a function of frequency can be given as

$$\varepsilon\left(\omega\right) = 1 + i\frac{\sigma_g\left(\omega\right)}{t_g\varepsilon_0\omega} \tag{6}$$

III. Unit Cell Design and Working Principle

The schematic view of the proposed multi-functional reflective type polarization converter is shown in Fig. 1. The metasurface is consist of 5 × 5 unit cell, capable of reflecting the vertically polarized incident EM wave to linearly or circularly polarized EM wave. The unit cell of the proposed metasurface based polarization converter is shown in Fig. 2. The unit cell consist of graphene layer on the top with symmetrical L-shaped pattern perforated on it. The middle layer is substrate SiO $_2$ with thickness 10 μm and backed with a bottom layer of gold with thickness 1 μm and conductivity 4.56 × 10^7 S/m. The design parameter of the proposed unit cell are determined after a comprehensive study of the reflection coefficients and phases of the EM wave at different values of chemical potential and scattering time constants. The optimized value of the design parameters are $l_1 = 1.37$ μm, $l_2 = 0.6$ μm, $w_1 = 0.26$ μm, $w_2 = 0.15$ μm, and $p = 3.25$ μm.

The unit cell is simulated in a commercially available software CST Microwave Studio, using full wave EM solver. Unit cell boundary conditions are given in x and y direction of the unit cell and Floquet mode excitation is given at top and bottom of the unit cell at λ/4 distance away. Initially, the chemical potential of the graphene is kept at 0.45 eV. The incident wave is considered to be y-polarized and coming from +z-direction. The wave is

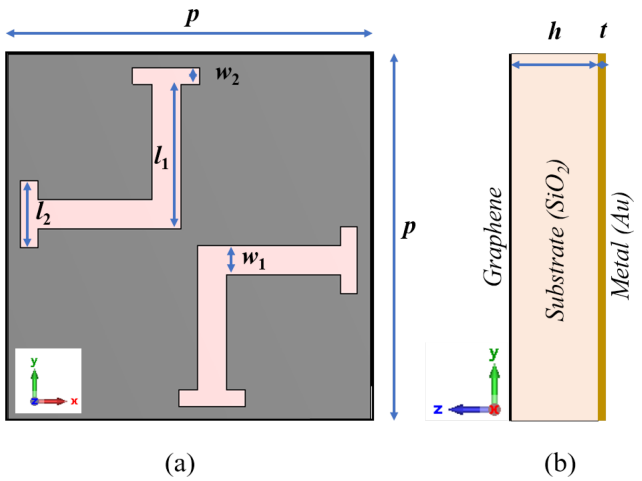

Fig. 2. Design of unit cell. (a) Top view of the unit cell. (b) Side profile of the unit cell operating in mid-Terahertz frequency band.

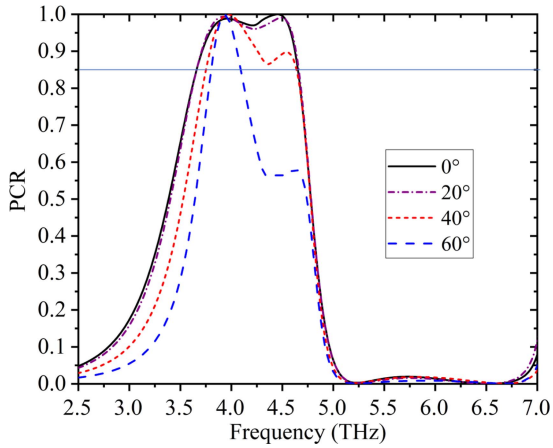

Fig. 4. PCR of the proposed metasurface under linearly polarized wave with different angle of incident at Fermi level 0.45 eV.

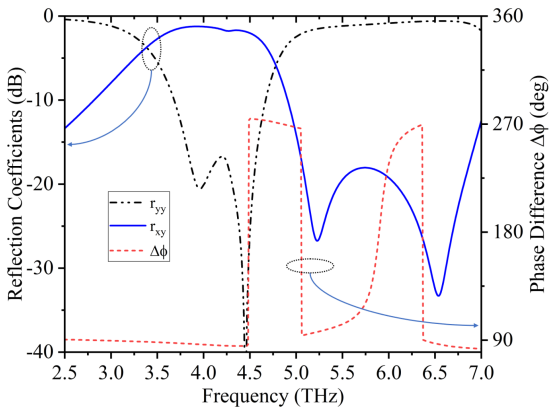

Fig. 3. Reflected co– and cross–polarized coefficient and phase difference at Fermi level 0.45 eV.

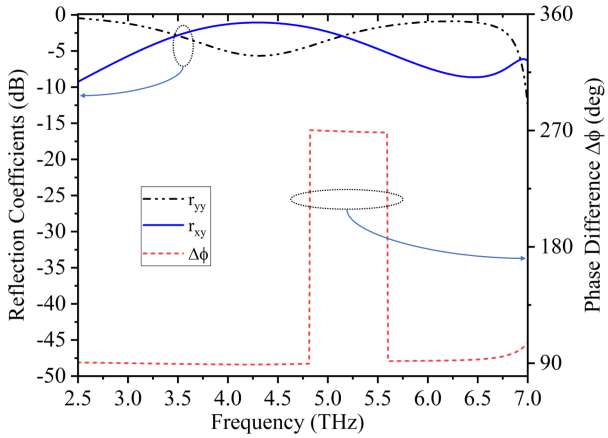

Fig. 5. Magnitude of the co- and cross-polarized reflection coefficient and their phase difference at Fermi level 0.9 eV.

reflected in +z-direction and the x-polarized and y-polarized reflection magnitudes are denoted as r_{xy} and r_{yy}, which are termed as cross-polarized and co-polarized reflections, respectively. The magnitude of the reflections coefficient of co- and cross-polarized wave and phase difference between them are shown in Fig. 3. From the figure it can be evident that the co polarized reflection coefficient is below -10 dB over the frequency band from 3.6 THz to 4.7 THz and the phase difference between them is odd multiple of $\pm 90^\circ$. From the figure, it can also be seen that there is an insertion loss of around 1 dB. This is due to the graphene layer has some conductive loss and multiple reflections of the wave in the substrate, between ground metallic layer and graphene layer is also responsible for this loss. Fig. 4 shows the polarization conversion ratio (PCR) of the proposed graphene based polarization conversion metasurface with change in the incident angle. At normal incident the fractional bandwidth is 31% for PCR more than 85%. The incident angle is changed from 0° to 60°, it is found that the PCR is above 0.85 upto the incident angle of 40°, reveals a good LL polarization conversion. The substrate's corresponding thickness from the incident wave's point of view increases with angle, which is the primary factor contributing to the PCR's decline at high frequencies and a decrease in performance. Nonetheless, the degradation is visible at roughly 4.5 THz when the oblique incident wave notices the shortening of one arm of the L-shaped perforated patches.

The PCR can be calculated using reflected co– and cross–polarized reflection coefficients' magnitude and phase. The PCR can be calculated by:

$$\text{PCR} = \frac{|r_{xy}|^2}{|r_{yy}|^2 + |r_{xy}|^2} \tag{7}$$

where, $|r_{yy}|$ and $|r_{xy}|$ are the co-polarized and cross-polarized coefficients of reflected wave. Further, the value of chemical potential is changed to 0.9 eV. The co and cross polarized reflection coefficients and the phase difference between them is shown in Fig. 5. From the figure, it is evident that they are almost equal to -3 dB and the phase difference is odd multiple of $\pm 90^\circ$ with small variation in the frequency range from 2.9 THz to 6.9 THz.

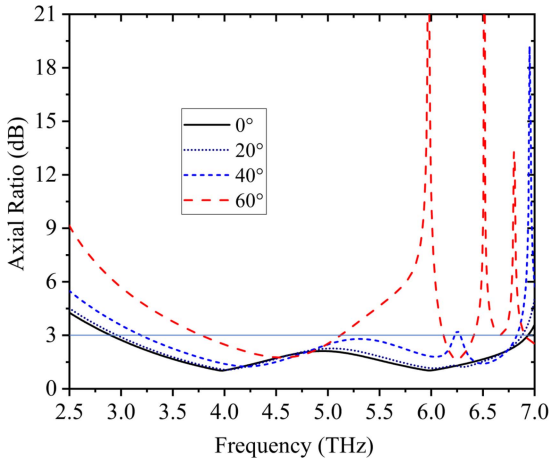

Fig. 6. AR with change in inclination angle of the linearly polarized incident wave at Fermi level 0.9 eV.

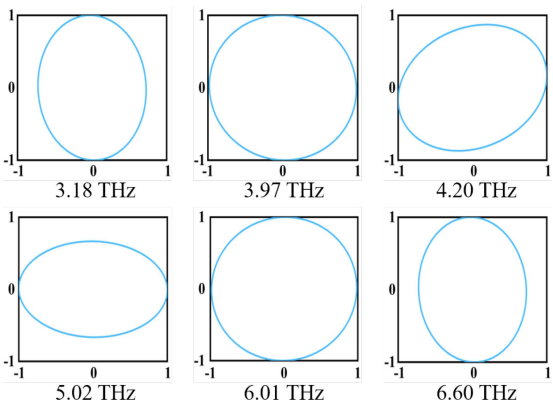

Fig. 7. Polarization Ellipses of the reflected circularly polarized EM wave upon linearly polarized incident, $E_f = 0.9$ eV.

From the magnitude and phase response, the AR can easily be calculated by using:

$$\text{Axial Ratio} = \sqrt{\frac{(|r_{yy}|^2 + |r_{xy}|^2 + \sqrt{\alpha})}{(|r_{yy}|^2 + |r_{xy}|^2 - \sqrt{\alpha})}} \tag{8}$$

where, $\alpha = |r_{yy}|^4 + |r_{xy}|^4 + 2|r_{yy}|^2|r_{xy}|^2 cos(2\Delta\phi)$. $\Delta\phi$ is the corresponding phase difference between the co-polarized and cross-polarized reflected EM wave.

The axial ratio of the reflected wave is shown in Fig. 6. At normal incident, the axial ratio is below 3 dB over 2.9 THz to 6.9 THz with the fractional bandwidth of 81% with respect to the center frequency. Further, the incident angle is changed from 0° to 60°, the axial ratio is maintained below 3 dB over the range of 3.2 THz to 6.7 THz upto the incident angle of 40°. As the incident angle increases the AR starts worsening at higher frequencies. The reason of deterioration of AR is same as discussed for the LL polarization conversion. For additional confirmation of the accuracy of polarization of the reflected electromagnetic wave, the polarization ellipses have been drawn in Fig. 7 at various frequencies. The figure shows that the reflected wave is circularly polarized when the axial ratio approaches 0 dB.

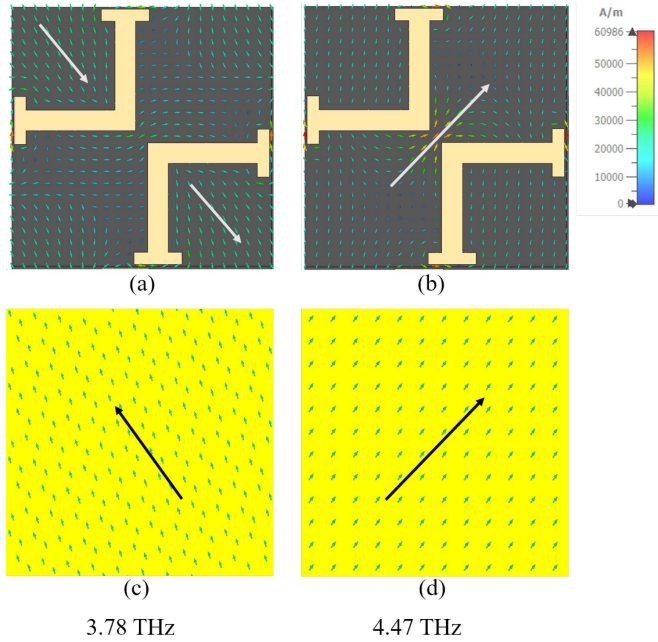

Fig. 8. Surface current distribution of the proposed metasurface unit cell at the top (a) & (b) and bottom (c) & (d) at resonance frequencies 3.78 THz and 4.47 THz, respectively for Fermi level 0.45 eV.

The equation for incident and reflected EM waves can be represented as $\vec{E_i} = (E_{iy})e^{jkz}$ and $\vec{E_r} = \binom{E_{ry}}{E_{rx}}e^{-jkz}$. The linear reflection matrix is given by:

$$\begin{pmatrix} E_{rx} \\ E_{ry} \end{pmatrix} = R_{ll}\,(E_{iy}) = \begin{pmatrix} r_{xy} \\ r_{yy} \end{pmatrix}(E_{iy}) \tag{9}$$

For the linearly polarized incident wave, the circularly polarized reflected wave can be expressed as

$$\begin{pmatrix} E_+^r \\ E_-^r \end{pmatrix} = \begin{pmatrix} E_{rx} + jE_{ry} \\ E_{rx} - jE_{ry} \end{pmatrix} = R_{cl}\,(E_{iy}) \tag{10}$$

$$R_{cl} = \begin{pmatrix} r_{+y} \\ r_{-y} \end{pmatrix} = \frac{1}{\sqrt{2}} \begin{pmatrix} r_{xy} + ir_{yy} \\ r_{xy} - ir_{yy} \end{pmatrix} \tag{11}$$

where, the subscripts + and - represents the left hand and right hand polarization of the reflected wave. The linear to circular reflection matrix contains the coefficients, which are responsible for the polarization of the EM wave. To obtain the circular polarization, one circularly polarized wave is much greater (or smaller) than the other one, i.e. $r_{+y} >> r_{-y}$ or $r_{-y} >> r_{+y}$.

IV. Results and Discussions

The behavior of the polarization converter can easily be analyzed with the help of incident and reflected EM wave at resonant frequencies. The two components $u-$and $v-$, are decomposed field of incident electric field. In the $u-$direction, as shown in Fig. 8(a) and (b) at resonance frequency 3.78 THz, the top surface current (Fig. 8(a)) and bottom surface currents (Fig. 8(b)) are anti-parallel, resulting in magnetic dipole along $v-$direction. As a result, the permeability of the electric field become higher

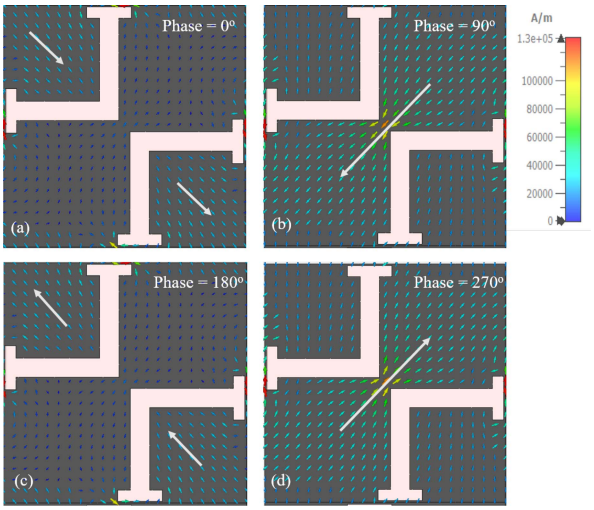

Fig. 9. Inducde surface current on the top of proposed metasurface unit cell corresponding to different phases at 3.97 THz: (a) 0°, (b) 90°, (c) 180°, and (d) 270°.

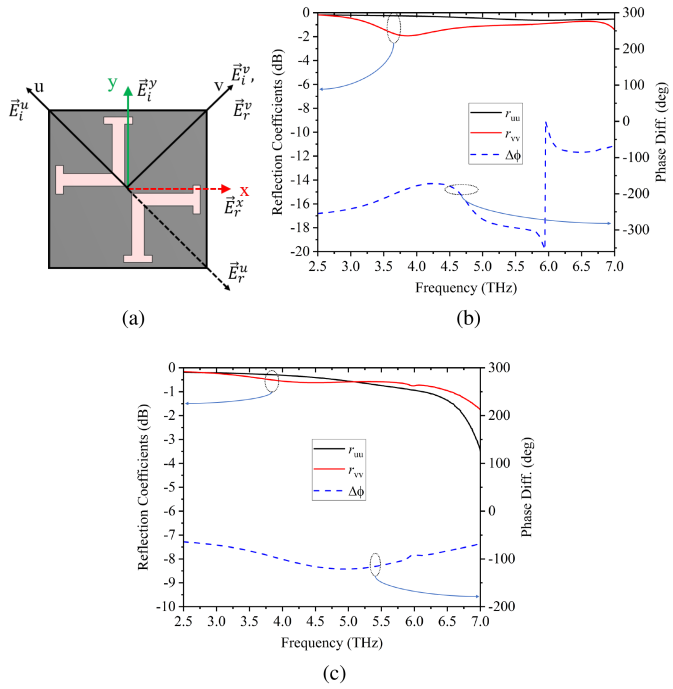

Fig. 10. (a) Unit cell under $u-$ and $v-$ polarized incidences (b) $u-$ and $v-$ polarized reflection coefficients and their phase difference at $E_f = 0.5$ eV and (c) at $E_f = 0.9$ eV.

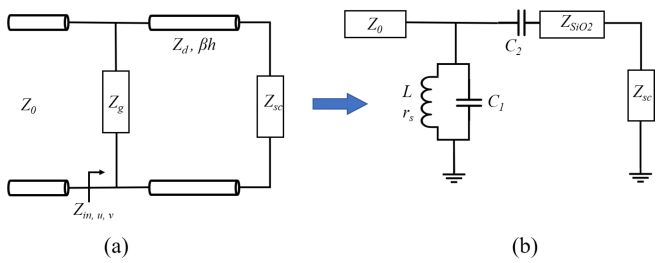

Fig. 11. (a) Schematic transmission line model of the proposed metasurface unit cell (b) Circuit model approach of the the proposed metasurface unit cell for u- and v- polarized incident wave at Fermi level 0.9 eV.

resulting in a high surface impedance and the reflected E-field is out of phase to the incident E-field for $v-$ polarized incident. However, the reflected field in the $u-$direction is along the incident field. The reflected $x-$polarized wave is produced by the synthesized reflected field. The top surface current (Fig. 8(c)) and bottom surface current (Fig. 8(d)) are parallel along $v-$direction at resonant frequency 4.47 THz, forming a electric dipole resonance in $v-$direction. This causes the resultant reflected electric field in $x-$direction.

The circular polarization and its behavior can be observed in Fig. 9. Upon different incident phase of the linearly polarized wave, the orientation of resultant current represented by white arrow, at resonant frequency 4 THz, is observed. The phase is changed from 0° to 270°. The current is progressively changing its direction in clockwise direction. This represents LHCP behavior of the reflected wave.

The incident electric field E_i can be decomposed into two orthogonal components along u and v axis, viz. E_{iu} and E_{iv}, shown in Fig. 10(a). Then the incident wave can be given as: $E_i = E_{iu} + E_{iv}$. As the unit cell is symmetric along u and v axis, thereby under $u-$ and $v-$ polarized incident electric field, there will be only co-polarized reflection coefficients.

$$E_r = E_{ru} + E_{rv}$$
$$E_r = r_{uu}E_{iu} + r_{vv}E_{iv} \tag{12}$$

where, r_{uu} and r_{vv} are the reflection coefficients along u and v axis under $u-$ and $v-$polarized incidences, respectively. The proposed unit cell is symmetric, so the reflection coefficients r_{uu} and r_{vv} are nearly equal in magnitude with phase difference $\Delta\phi$ over the frequency or $r_{uu} = r_{vv}e^{j\Delta\phi}$. Then (IV) can be written as:

$$E_r = r_{vv}e^{j\Delta\phi}E_{iu} + r_{vv}E_{iv} \tag{13}$$

If the value of phase difference $|\Delta\phi| = 180°$, the resultant reflected electric field of the components E_{ru} and E_{rv} is orthogonal to the incident electric field E_i. So the reflected wave is $x-$polarized. If $|\Delta\phi| = 90°$, the reflected wave components E_{ru} and E_{rv} are out of phase by $\pi/2$, and a reflected circularly polarized wave is formed.

The equivalent circuit diagram is given in Fig. 11 to observe the operation of the proposed device in LC polarization mode. The characteristic impedance of free space and the substrate are given as Z_o and Z_d, respectively. The metal layer at the bottom of the unit cell is represented as short circuit impedance. The anisotropic top graphene layer's tensor sheet impedance is denoted by Z_g [28]. It exhibits a distinct impedance for u and v polarized occurrences because of the anisotropy of the top layer. The u and v polarized wave is illuminated on a free-standing top layer in order to determine the sheet impedance of the top layer for u and v polarization. Further, full wave EM simulation is performed using CST microwave studio to extract the sheet impedance as shown in Fig. 12. To eliminate the circuit effect

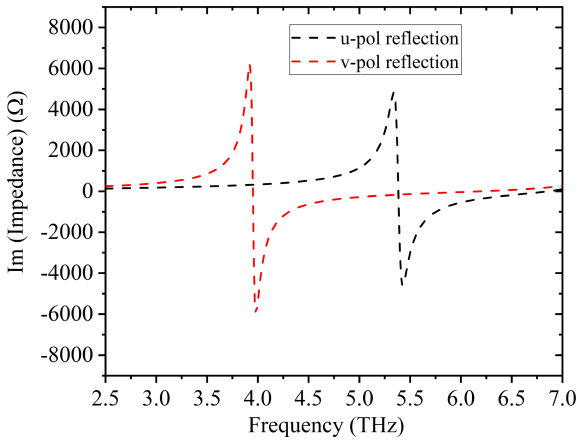

Fig. 12. Extracted sheet impedances of the metasurface under u- and v-polarized incident wave.

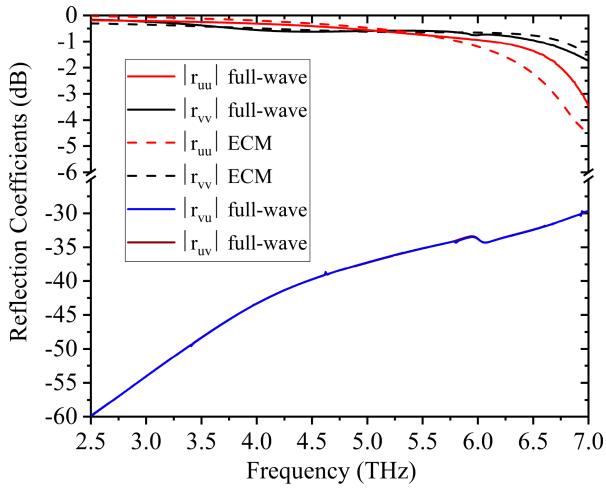

Fig. 13. Reflection coefficients of the ECM simulation compared with the Full wave simulation for $u-$ and $v-$components of the y-polarized incident wave.

which is phase in our case, due to distant port at the input, we de-embedded the port to the top surface of unit cell. Moreover, an equivalent circuit model is drawn by examining the geometry of the unit cell and the extracted sheet impedance. A resonance that can be detected in the extracted sheet impedance under both u and v polarized occurrences indicates a parallel LC circuit. Therefore, for u and v polarized incidences the equivalent circuit diagram is similar with different parameter values as shown in Fig. 11(b). The resistive element (r_s) has been incorporated to address the losses resulting from the periodic slotting of graphene metasurface. The coupling capacitance (C_2) between the bottom gold layer and the top graphene metasurface is also included in the circuit model. Since the graphene layer on the SiO_2 substrate is continuous, the parasitic capacitance is not considered. The parameters of the designed circuit diagram is further optimized to map with the full wave simulation result, the value of circuit parameters for u-polarized incidence are given as $L_u = 3.2\,pH$, $C_{u1} = 2.29\,fF$, $r_{us} = 0.71\,\Omega$ and $C_{u2} = 0.86\,fF$. For v-polarized incidence the optimized equivalent circuit diagram is given as $L_v = 3.11\,pH$, $C_{v1} = 1.5\,fF$, $r_{vs} = 0.72\,\Omega$, and $C_{v2} = 0.86\,fF$. The reflection coefficients of the two orthogonal polarized incident wave under full wave simulation and equivalent circuit model is shown in Fig. 13. The cross polarized reflection coefficients are also shown in the figure which is very low. From this, it is evident that the coupling between u and v components is very low. The results show that there is a strong agreement between the full wave simulated results and the ECM results.

Altering the Fermi level across the graphene layer and bottom gold by external biasing or doping leads to change in the surface conductivity given by 2. To observe the operating range of the proposed device, the Fermi level has been varied. From the Fig. 14, it can be seen that the Fermi level varied from 0.3 eV to 0.6 eV. The PCR is above 90% for 0.4 eV to 0.5 eV. Further, the Fermi level is altered from 0.7 eV to 1.0 eV, the AR is calculated from the reflection coefficients using 8 is drawn in Fig. 15. We have investigated the results for chemical potential upto 1 eV, as beyond this practically not realized till date [29].

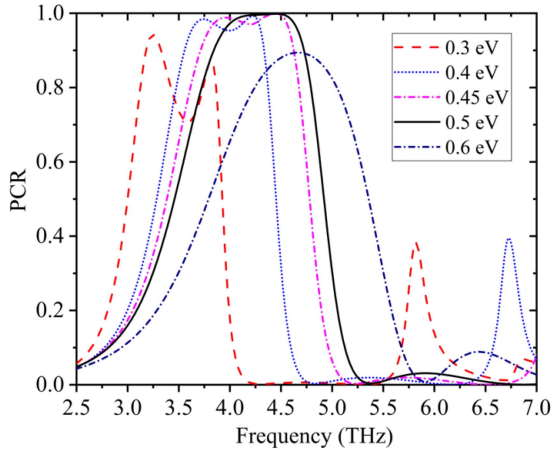

Fig. 14. Change in PCR of the proposed graphene based metasurface with altering the chemical potential across graphene and bottom gold from 0.3 eV to 0.6 eV.

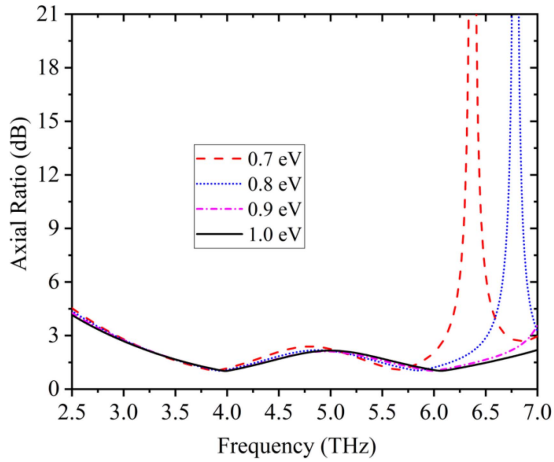

Fig. 15. AR of the reflected circularly polarized wave by altering the the chemical potential across graphene and bottom gold layer from 0.7 eV to 1.0 eV.

TABLE I
COMPARISON OF THE PROPOSED DESIGN WITH OTHER POLARIZATION CONVERTERS

Polarization Converter	Configuration	Fractional Bandwidth	Thickness	Angular stability(°)	Active Parameters
[26]	Si Graphene PMMA Metal	LC-20% LL-9.5%	λ/2.8	NR	Chemical Potential
[27]	Graphene-SiO_2-Metal	LC-3% LL-3%	λ/4.5	NR	Chemical Potential
[16]	Metal-Graphene-SiO_2 -Neltec NY 9208-Metal	LC-42.3% LL-22%	λ/6.2	Up to 12.5	Chemical Potential
[19]	Graphene-SiO_2-Metal	LC-37% LL-73%	λ/4.3	Up to 35-TM 25-TE	Chemical Potential
[12]	VO_2-Graphene-COC VO_2-Graphene-VO_2 COC-Graphene	LC-54% LL-103% (Transmissive)	λ/4.1	Up to 40	Chemical Potential Temperature
[17]	Graphene-SiO_2-VO_2-Metal	LL-66%(Transmissive) LL-10% (Reflective)	λ/9.5	NR	Chemical Potential Temperature
Our design	Graphene-SiO_2-Metal	LC-81% LL-31%	λ/7.5	Up to 40	Chemical Potential

Further, the proposed graphene based multi-function metasurface polarization converter is compared with the available multi-function polarization converter. Although, there are literature available related to polarization converter, we have compared a few on them. The limitation with the other structure is that they have more than one parameter to achieve the multi-functional polarization conversion. Even if one parameter is used in that case, the structure is multi-layer with narrow band response. From the comparison Table I, It is evident that, in the case of LC polarization conversion, the bandwidth of the proposed device is better than that found in the literature.. Moreover, from the fabrication and switching point of view, the complexity of the proposed structure is very less than the available.

V. CONCLUSION

In the forgoing, a reconfigurable broadband polarization conversion metasurface is proposed. By altering the Fermi level of the single layered graphene, the reflected polarization characteristic of the metasurface is changed from LL to LC polarization converter. It gives LL polarization conversion with 31% fractional bandwidth for 0.3 eV to 0.6 eV. On the other hand, it gives LC polarization with maximum fractional bandwidth of 81% for Fermi level of 0.7 to 1.0 eV. The current distribution and polarization ellipses are drawn to show the polarization conversion. The equivalent circuit diagram is also drawn to support the fact. The results of ECM are in good agreement with the full wave simulated results. The device finds application in switching devices, polarization manipulation of THz waves.

REFERENCES

[1] M. Feng, J. Wang, H. Ma, W. Mo, H. Ye, and S. Qu, "Broadband polarization rotator based on multi-order plasmon resonances and high impedance surfaces," *J. Appl. Phys.*, vol. 114, no. 7, 2013, Art. no. 074508.

[2] H. Cheng et al., "Dynamically tunable broadband mid-infrared cross polarization converter based on graphene metamaterial," *Appl. Phys. Lett.*, vol. 103, no. 22, 2013, Art. no. 223102.

[3] N. K. Grady et al., "Terahertz metamaterials for linear polarization conversion and anomalous refraction," *Science*, vol. 340, no. 6138, pp. 1304–1307, 2013.

[4] X. Gao, X. Han, W.-P. Cao, H. O. Li, H. F. Ma, and T. J. Cui, "Ultrawideband and high-efficiency linear polarization converter based on double v-shaped metasurface," *IEEE Trans. Antennas Propag.*, vol. 63, no. 8, pp. 3522–3530, Aug. 2015.

[5] P. C. Wu et al., "Broadband wide-angle multifunctional polarization converter via liquid-metal-based metasurface," *Adv. Opt. Mater.*, vol. 5, no. 7, 2017, Art. no. 1600938.

[6] N. I. Landy, S. Sajuyigbe, J. J. Mock, D. R. Smith, and W. J. Padilla, "Perfect metamaterial absorber," *Phys. Rev. Lett.*, vol. 100, no. 20, 2008, Art. no. 207402.

[7] R. Agrahari et al., "Triple-band metasurface absorber for RF energy harvesting applications," *Microw. Opt. Technol. Lett.*, vol. 65, pp. 2252–2261, 2023.

[8] J. Li, Y. Yuan, Q. Wu, and K. Zhang, "Bi-isotropic Huygens' metasurface for polarization-insensitive cross-polarization conversion and wavefront manipulation," *IEEE Trans. Antennas Propag.*, vol. 72, no. 3, pp. 2445–2454, Mar. 2024.

[9] H. Yang, S. C. Wang, P. Li, Y. He, and Y. J. Zhang, "Broadband multifunctional reconfigurable polarization conversion metasurface," *IEEE Trans. Antennas Propag.*, vol. 71, no. 7, pp. 5759–5767, Jul. 2023.

[10] M. Saikia, S. Ghosh, and K. Srivastava, "Switchable reflective metamaterial polarisation rotator," *Electron. Lett.*, vol. 52, no. 12, pp. 1030–1032, 2016.

[11] Z. Tao, X. Wan, B. C. Pan, and T. J. Cui, "Reconfigurable conversions of reflection, transmission, and polarization states using active metasurface," *Appl. Phys. Lett.*, vol. 110, no. 12, 2017, Art. no. 121901.

[12] X. Zhang, K. Zhang, B. Chen, L. Guo, and W. Kong, "Switchable multifunctional broadband polarization converter in terahertz band," *Opt. Exp.*, vol. 30, no. 23, pp. 41969–41979, 2022.

[13] S. Mikhailov, *Physics and Applications of Graphene: Experiments*. Rijeka, Croatia: InTech, 2011.

[14] V. S. Yadav, S. K. Ghosh, S. Bhattacharyya, and S. Das, "Graphene-based metasurface for a tunable broadband terahertz cross-polarization converter over a wide angle of incidence," *Appl. Opt.*, vol. 57, no. 29, pp. 8720–8726, 2018.

[15] V. S. Yadav, B. K. Kaushik, and A. Patnaik, "Broadband THz absorber for large inclination angle TE and TM waves," *IEEE Photon. J.*, vol. 13, no. 5, Oct. 2021, Art. no. 7700107.

[16] J. Zhang, K. Zhang, A. Cao, Y. Liu, and W. Kong, "Bi-functional switchable broadband terahertz polarization converter based on a hybrid graphene-metal metasurface," *Opt. Exp.*, vol. 28, no. 18, pp. 26102–26110, 2020.

[17] Z. Xiao, X. Jiang, X. Wang, and Z. Cui, "Switchable polarization converter with switching function based on graphene and vanadium dioxide," *J. Electron. Mater.*, vol. 52, no. 3, pp. 1968–1976, 2023.

[18] G. Ding, Y. Zhou, S. Zhang, X. Luo, and S. Wang, "Design of a reconfigurable ultra-wideband terahertz polarization rotator based on graphene metamaterial," *Sensors*, vol. 23, no. 12, 2023, Art. no. 5449.

[19] R. Zhang, B. You, S. Wang, K. Han, X. Shen, and W. Wang, "Broadband and switchable terahertz polarization converter based on graphene metasurfaces," *Opt. Exp.*, vol. 29, no. 16, pp. 24804–24815, 2021.

[20] Y. Zhang, Y. Feng, B. Zhu, J. Zhao, and T. Jiang, "Switchable quarter-wave plate with graphene based metamaterial for broadband terahertz wave manipulation," *Opt. Exp.*, vol. 23, no. 21, pp. 27230–27239, 2015.

[21] Y.-Y. Ji, F. Fan, X.-H. Wang, and S.-J. Chang, "Broadband controllable terahertz quarter-wave plate based on graphene gratings with liquid crystals," *Opt. Exp.*, vol. 26, no. 10, pp. 12852–12862, 2018.

[22] J. Pang et al., "Self-terminating confinement approach for large-area uniform monolayer graphene directly over Si/SiO_x by chemical vapor deposition," *ACS Nano*, vol. 11, no. 2, pp. 1946–1956, 2017.

[23] Y. Zhang, L. Zhang, and C. Zhou, "Review of chemical vapor deposition of graphene and related applications," *Accounts Chem. Res.*, vol. 46, no. 10, pp. 2329–2339, 2013.

[24] J. T. Kim, H. Choi, Y. Choi, and J. H. Cho, "Ion-gel-gated graphene optical modulator with hysteretic behavior," *ACS Appl. Mater. Interfaces*, vol. 10, no. 2, pp. 1836–1845, 2018.

[25] G. W. Hanson, "Dyadic Green's functions and guided surface waves for a surface conductivity model of graphene," *J. Appl. Phys.*, vol. 103, no. 6, 2008, Art. no. 064302.

[26] S. Guan, J. Cheng, T. Chen, and S. Chang, "Bi-functional polarization conversion in hybrid graphene-dielectric metasurfaces," *Opt. Lett.*, vol. 44, no. 23, pp. 5683–5686, 2019.

[27] H. Zhang et al., "Multi-functional polarization conversion manipulation via graphene-based metasurface reflectors," *Opt. Exp.*, vol. 29, no. 1, pp. 70–81, 2021.

[28] B. O. Zhu, "Metasurface synthesis with arbitrary incident angles using planar electric impedance surfaces," *IEEE J. Multiscale Multiphys. Comput. Tech.*, vol. 4, pp. 51–56, 2019.

[29] G. Klimchitskaya, V. Mostepanenko, and V. Petrov, "Impact of chemical potential on the reflectance of graphene in the infrared and microwave domains," *Phys. Rev. A*, vol. 98, no. 2, 2018, Art. no. 023809.